Compositional Variation in Hydrocarbon Reservoirs with Natural Convection and Diffusion

Mike F. Riley and Abbas Firoozabadi
Reservoir Engineering Research Institute, Palo Alto, CA 94304

The knowledge of horizontal compositional variation is of prime importance in hydrocarbon reservoir delineation. However, the effect of natural convection on this variation is largely unknown. This work examines the effect of natural convection and diffusion (thermal, pressure and Fickian) on a two-component, single-phase fluid occupying a horizontal cross-sectional reservoir in the presence of a prescribed linear temperature field. The behavior is investigated using a method of successive approximations, which iterates on solution of Poisson's equation. This behavior is then incorporated in a simplified perturbation solution (in the form of a cubic equation) which not only gives accurate values of horizontal compositional variation, but also clearly shows the interplay of reservoir/fluid properties. The perturbation and the full solutions indicate that a small amount of convection can cause the horizontal composition gradients to increase until a maximum is reached and then decay as 1/k. An alternative scenario is that the gradient asymptotes to a value where the horizontal density derivative approaches zero. Generalization of this perturbative solution to n-components apparently requires the simultaneous solution of $n-1$ cubic equations.

Introduction

Compositional variation in hydrocarbon reservoirs plays an important role in reservoir delineation. The ability to predict horizontal compositional variation helps the engineer to determine whether a given pair of producing wells drain the same reservoir. However, prior to this study the effects of natural convection on this horizontal variation were largely unknown, and many *a-priori* suppositions turned out to be wrong. The primary goal of this work was to achieve an understanding of the effects of natural convection and diffusion (molecular, pressure and thermal) on horizontal compositional variation.

There is a substantial body of work investigating the combined effects of diffusion and natural convection. However, the vast majority of that research investigates the onset of convection due to vertical instabilities; the cases considered are where convection results solely from vertical geothermal gradients high enough to generate instabilities and induce stable convection. (For an application to hydrocarbon reservoirs see Bedrikovetskii, Polonskii, and Shapiro (1993).) That type of investigation is only distantly related to our work. In this work, we consider that thermal convection results from a horizontal component of the local geothermal gradient and are unconcerned with the stability question.

To our knowledge, the main work on compositional variation in petroleum reservoirs with free convection due to imposed horizontal temperature gradients is by Jacqmin (1986, 1990) and Moser (1986). These authors are concerned with a wide variety of conditions: multicomponents (that is, more than two), unsteady-state conditions, sloping reservoirs, and even two phases. However, neither author includes thermal diffusion. Moser employs finite-difference reservoir simulation (which seems to work well), while Jacqmin uses a perturbative-type approach where approximations are made to the governing equations. These authors state that under certain conditions the fluid composition reorients itself in such a way as to inhibit convection—we discuss this point in detail later. Both authors develop simplified expressions (essentially quadratic equations) to model horizontal compositional variation—we discuss Jacqmin's later.

Our treatment is more focused and systematic because of great subtleties of this problem. We are concerned that either finite-difference simulation or direct perturbation analy-

Correspondence concerning this article should be addressed to A. Firoozabadi.

sis (using *a-priori* assumptions of dominant behavior) would mask important phenomenon. In this work the problem is developed in three stages: first, we attempt to get accurate results for the two-component single-phase case, second, we examine these results to develop an understanding of the dominant phenomena, and third, we incorporate these dominant behaviors into simplified solutions. We desire to find the dependence of the solution on all of the parameters in the equations; thus, we seek solution to the differential equations including all of the fluid property variation. Finally, we make heuristic arguments for extending the perturbation solutions to multicomponent systems.

Governing Differential Equations

Here we present the differential equations that govern the two-component convection/diffusion problem. The equations are simply an expression of the conservation of mass. We assume that the fluid flow is steady, and that the reservoir is a two-dimensional vertical rectangle (that is, $x-z$). The fluid consists of two components and is a single-phase liquid or gas. We also assume that we know the temperature field in order to obviate the solution of the conservation of energy equation.

In the steady state, the conservation of mass for the bulk fluid can be written

$$\nabla\cdot(\rho\vec{v})=0, \tag{1}$$

where ρ is the mass density of the bulk fluid, and $\vec{v}$ is the total velocity. The unknowns in this equation are composition (that is, the mole or mass fraction of one of the components), and pressure. In order to constrain these two quantities, we must solve this equation together with a second equation expressing conservation of mass of component one

$$\nabla\cdot\left(\omega\rho\vec{v}+\vec{j}\right)=0. \tag{2}$$

Here ω and $\vec{j}$ are the weight fraction and diffusive-mass flux of component one. The diffusive flux $\vec{j}$ results from the deviation in the velocity of component one from the velocity of the bulk fluid. Since, in the case of a two-component system, the diffusive flux of component two is equal to $-\vec{j}$ and the weight fraction of component two is equal to $1-\omega$, a third equation written for component two will be a linear combination of the previous two equations and, hence, superfluous.

In Eqs. 1 and 2, we assume that the velocity $\vec{v}$ is given by Darcy's law

$$\vec{v}=-\frac{k}{\varphi\mu}(\nabla P+\rho g\hat{z}), \tag{3}$$

where g is the acceleration due to gravity, k is the permeability, φ is the porosity, and μ is fluid viscosity. The unit vector $\hat{z}$ points upwards.

The diffusive flux of component one is given by the expression (Bird et al., 1960)

$$\vec{j}=C^{\chi}(\chi,P,T)\nabla\chi+C^{P}(\chi,P,T)\nabla P+C^{T}(\chi,P,T)\nabla T. \tag{4}$$

The coefficients in this expression are

$$C^{\chi}=-\rho\frac{d\omega}{d\chi}D_{12}\left(\frac{\partial\ln f}{\partial\ln\chi}\right)_{T,P},$$

$$C^{P}=-\rho\frac{d\omega}{d\chi}D_{12}\frac{\chi}{RT}\left(\bar{V}_1-\frac{M_1}{\rho}\right),$$

$$C^{T}=-\rho\frac{d\omega}{d\chi}D_{12}\frac{k_T}{T}, \tag{5}$$

where D_{12} is the diffusion coefficient, f is the fugacity of component one, $\bar{V}_1$ is the partial molar volume of component one, R is the gas constant, k_T is the thermal diffusion ratio, and χ is the mole fraction of component one. The mole fraction χ and the mass fraction ω are related to each other by the expression: $\omega=\chi M_1/[\chi M_1+(1-\chi)M_2]$, where M_1 and M_2 are the molecular weights. All of the other quantities in these expressions are readily calculated using an equation of state, except D_{12} and k_T.

For the present, we assume that D_{12} is constant; in our examples, we take a representative value of D_{12} from Sigmund (1976) and adjust it for porous media by dividing by the product of electrical resistivity factor and fractional porosity (Perkins and Johnston, 1963). The thermal diffusion ratio k_T is estimated using an approximation given by Rutherford and Roof (1959) for methane/normal butane systems

$$k_T=-82{,}600\frac{\chi(1-\chi)}{RT}. \tag{6}$$

The ratio k_T is dimensionless and the coefficient 82,600 is for R having units of atm·cm^3/mol·K, and T in degrees Kelvin. We did not modify k_T from the above equation for nonideal fluid behavior (see the discussion by Shukla and Firoozabadi, 1997).

The boundary conditions for Eqs. 1 and 2 are that no fluid crosses the outer boundaries

$$j_x=\rho v_x=0, \qquad x=\pm W/2,$$

$$j_z=\rho v_z=0, \qquad z=\pm H/2, \tag{7}$$

where the subscripts x and z refer to horizontal and vertical directions, and H and W are the height and width of the reservoir.

We require two other pieces of information in order to set the composition and pressure levels. There are a few ways to do this. For instance, one could set average values over the reservoir. In this work, we assign a pressure and composition at one point (taken for convenience to be the origin), because it is the information obtained from a well.

Energy Equation

Here we briefly discuss the energy equation that governs the temperature field. We do not include this equation in our calculations, because we assign a temperature field.

If we assume that a single-phase fluid flows at steady conditions and neglect the interdiffusion contribution in porous media, the temperature field must satisfy

$$\nabla\cdot(K\nabla T)-\rho\vec{v}c_p\nabla T=0. \tag{8}$$

In the above equation, K is the thermal conductivity, the first term is the conductive energy flux, and the second term is the convective energy flux.

We do not solve this equation simply, because it would unduly complicate the problem. Temperature data in a petroleum reservoir can be measured with modern tools, which are much easier than composition measurements. Oil field temperature data indicate linear horizontal temperature variation.

We assume that our reservoir is bounded by rock that has constant temperature gradients T_x and T_z in horizontal and vertical directions with $T_x \ll T_z$. This is a good assumption when the Peclet number is $\ll 1$. We also assume that the conductive flow of heat in our reservoir is much greater than the convective flow. With these assumptions, the solution of Eq. 8 will have roughly the same temperature gradients as the bounding rock.

Iterative Procedure

Initially, we held the notion that the compositional gradients should be monotonic functions of position (that is, that compositional gradients had no local maxima or minima within the reservoir). We also assumed that compositional gradients would decrease monotonically with increasing permeability. Aside from these two assumptions (which were wrong), we had little information on which terms in these equations would dominate and which could be neglected. This made a perturbation approach hard to justify. We also thought that a conventional finite-difference approach would be too crude for our purposes.

We decided to take advantage of the vector nature of the convective and diffusive fluxes by expressing them in terms of vector and scalar potentials (that is, in terms of their rotational and irrotational parts) and using a method of successive approximations. This approach had the advantage of being an exact representation for zero convection.

Vector Formulation

The Fundamental Theorem of Vector Analysis states that a continuous vector field with continuous divergence and curl can be represented by the sum of its rotational and irrotational parts (for example, Borisenko and Tarapov, 1979). For instance, the diffusion flux vector can be expressed as

$$\vec{j}=\left(\vec{j}\right)_{\mathrm{ROT}}+\left(\vec{j}\right)_{\mathrm{IRR}}. \tag{9}$$

These components are determined by the requirements that the divergence of the rotational part be zero and that the curl of the irrotational part be zero. Because these are properties held by the curl and gradient, respectively, we can represent the convection and diffusion mass fluxes of component one by (using Eq. 2)

$$\begin{aligned}\omega\rho\vec{v}&=\nabla\times(\psi_{v1}\hat{y})+\nabla\phi\\&=-\frac{\partial\psi_{v1}}{\partial z}\hat{x}+\frac{\partial\psi_{v1}}{\partial x}\hat{z}+\frac{\partial\phi}{\partial x}\hat{x}+\frac{\partial\phi}{\partial z}\hat{z},\\\vec{j}&=\nabla\times(\psi_j\hat{y})-\nabla\phi\\&=-\frac{\partial\psi_j}{\partial z}\hat{x}+\frac{\partial\psi_j}{\partial x}\hat{z}-\frac{\partial\phi}{\partial x}\hat{x}-\frac{\partial\phi}{\partial z}\hat{z}.\end{aligned} \tag{10}$$

where $\hat{x}$ and $\hat{y}$ are the unit vectors along the x and y axes, respectively.

The representation of the total mass flux is simpler. Since, the divergence of $\rho\vec{v}$ is zero and since the components of this vector normal to the boundary are zero, the irrotational part must be zero

$$\rho\vec{v}=\nabla\times(\psi\hat{y})=-\frac{\partial\psi}{\partial z}\hat{x}+\frac{\partial\psi}{\partial x}\hat{z}. \tag{11}$$

This is essentially the stream function used in fluid mechanics (for example, Lu, 1973).

The partial differential equations for ψ and ψ_j are derived by taking the curl of the vectors $\rho\vec{v}$ and $\vec{j}$ expressed in vector potential form and setting them equal to the curl of their definitions given in the previous section. We do not compute ψ_{v1} in this work.

The equation governing total mass flux is

$$\frac{\partial^2\psi}{\partial x^2}+\frac{\partial^2\psi}{\partial z^2}=-\frac{kg}{2\varphi\mu}\frac{\partial\rho^2}{\partial x}-\frac{\rho v_x}{2\rho^2}\frac{\partial\rho^2}{\partial z}+\frac{\rho v_z}{2\rho^2}\frac{\partial\rho^2}{\partial x}. \tag{12}$$

Note that in this equation we have implicitly assumed that viscosity is constant. This assumption has been made for convenience and should in no way limit the applicability of the method. We have also assumed that permeability and porosity are constant. This should not be overly restrictive, unless they vary wildly within the reservoir.

By far the most important term on the right side of Eq. 12 (at least away from $x=\pm W/2$) is the first (see Firoozabadi, 1998). If we include only this term and neglect the horizontal pressure gradient (which is extremely small for the ρ variation), we get

$$\frac{\partial^2\psi}{\partial x^2}+\frac{\partial^2\psi}{\partial z^2}\cong-\frac{kg}{2\varphi\mu}\left(\frac{\partial\rho^2}{\partial\chi}\frac{\partial\chi}{\partial x}+\frac{\partial\rho^2}{\partial T}\frac{\partial T}{\partial x}\right). \tag{13}$$

While we use the full equation in our iterative method, we use this approximation for the perturbation analysis.

The equation for the rotational part of the diffusive flux is

$$\begin{aligned}\frac{\partial^2\psi_j}{\partial x^2}+\frac{\partial^2\psi_j}{\partial z^2}=&-\frac{\partial\chi}{\partial x}\frac{\partial C^\chi}{\partial z}+\frac{\partial\chi}{\partial z}\frac{\partial C^\chi}{\partial x}-\frac{\partial T}{\partial x}\frac{\partial C^T}{\partial z}\\&+\frac{\partial T}{\partial z}\frac{\partial C^T}{\partial x}-\frac{\partial P}{\partial x}\frac{\partial C^P}{\partial z}+\frac{\partial P}{\partial z}\frac{\partial C^P}{\partial x}.\end{aligned} \tag{14}$$

Note that every term on the right side of this equation contains the derivative of a diffusion coefficient. Since these co-

efficients are slowly varying functions of pressure, temperature, and composition away from the critical point, we expect the contribution of ψ_j to be small.

The dependent variables ψ and ψ_j have constant values on the boundary. Without loss of generality, we assign these constants to be zero

$$\psi = \psi_j = 0, \qquad x = \pm W/2,$$
$$\psi = \psi_j = 0, \qquad z = \pm H/2. \tag{15}$$

There are a number of equivalent representations for the scalar potential ϕ. One representation uses the difference between $\omega\rho\vec{v}$ and its rotational part: $\nabla\phi = \omega\rho\vec{v} - (\omega\rho\vec{v})_{\mathrm{ROT}}$. This representation was tried and rejected, because it expresses the scalar potential as the difference between two nearly equal quantities. This is because the mass flux of component one due to convection is normally much larger than that due to diffusion. Note that the continuity equation for component one, Eq. 2, does not say that $\vec{j}$ is equal and opposite to $\omega\rho\vec{v}$. It says that the *irrotational part* of $\vec{j}$ is equal and opposite to the *irrotational part* of $\omega\rho\vec{v}$. This is an important point since the rotational part of $\omega\rho\vec{v}$ is often orders of magnitudes larger than its irrotational part; for $\vec{j}$ the converse is true.

To bring out the dependence of the scalar potential ϕ on variation in composition, we rewrite Eq. 2 using Eq. 1

$$\nabla^2\phi = \rho\vec{v}\cdot\nabla\omega\left(= -\nabla\cdot\vec{j}\right). \tag{16}$$

This form, however, makes the computation of ϕ sensitive to small errors in ω.

The boundary condition for this equation is that ϕ have zero normal derivatives on the boundary

$$\frac{\partial\phi}{\partial x} = 0, \qquad x = \pm W/2,$$
$$\frac{\partial\phi}{\partial z} = 0, \qquad z = \pm H/2. \tag{17}$$

As we see later, the dependent variables ψ and ϕ are related to velocity and composition, respectively.

Solution Mechanics

The differential equations of the previous section (Eqs. 12, 14 and 16) all have the general form

$$\nabla^2 F(x,z) = g(x,z). \tag{18}$$

This suggests an iterative scheme that assumes at each step we know the $g(x,z)$'s. The first step is to assume a pressure and composition distribution and use this to determine $\rho\vec{v}$ from Eq. 12. The mass flux field is then used to compute ϕ and ψ_j from Eqs. 14 and 16. Updated composition and pressure distributions are determined by integrating

$$\nabla\chi = \frac{-\nabla\phi + \nabla\times\psi_j\hat{y} - C^P\nabla P - C^T\nabla T}{C^\chi}, \tag{19}$$

together with Darcy's law.

Note that, aside from the integration, this procedure requires successive solution of Poisson's equation. So far, we have solved them by integration of the corresponding Green's function over the reservoir. Because we need the derivatives of ϕ, ψ and ψ_j with respect to x or z, we compute them directly by using the derivatives of the Green's functions in the integrals.

Each differentiated Green's function, except the one corresponding to $\partial\phi/\partial x$ has the form

$$\Sigma\,(\text{sine or cosine terms})\,(\text{exponential terms}). \tag{20}$$

The arguments of the trigonometric terms have the form $n\pi(\eta + H/2)/H$ and $2n\pi(z + H/2)/H$, while the exponentials have arguments for the source point, $-n\pi\,|(x-\xi)|/H$, and the images about the side boundaries. The variables ξ and η are the dummy variables of integration.

The differentiated Green's function for $\partial\phi/\partial x$ contains (in addition to a series of the type given) a Heaviside step function $H(x-\xi)$. Integration of this step function with respect to the dummy variables ξ and η over the rectangle shows that this part of $\partial\phi/\partial x$ is its value averaged over z from $-H/2$ to $+H/2$ and $\partial\bar{\phi}/\partial x$ can be expressed by

$$\frac{\partial\bar{\phi}}{\partial x} = \frac{1}{H}\int_{-H/2}^{H/2}\omega\rho v_x dz. \tag{21}$$

Equation 21 is obtained from Eqs. 1 and 6 and the appropriate boundary conditions.

We integrate the Green's function solutions by dividing the reservoir into small rectangles assuming that the forcing functions are constant in each rectangle. We integrate the differentiated Green's functions analytically and then multiply them by the averaged forcing function. The grid of rectangles is refined so that they are narrowest near the side boundaries and shortest at the top and bottom of the reservoir. The width of the rectangles near the side boundaries are decreased as permeability is increased.

Examples

In order to investigate the behavior of the binary system and to test the validity of the iterative procedure, we considered a binary mixture of methane and normal butane. The parameters for this example are given in Table 1; the thermodynamic properties are calculated using the Peng-Robinson (1976) equation of state. The nature of this system is that methane tends toward the hotter region because of thermal diffusion effects (see Shukla and Firoozabadi, 1997). This tendency overrides the buoyancy due to pressure effects, so that butane actually "floats" above the methane. Since we had convergence problems with this case, and in order to investigate the behavior when the lighter component concentrated at the top of the reservoir, we studied a second case where the sign of k_T was changed.

Table 1. Data for Binary Liquid Example

Thickness	H	150 m
Length	W	3,000 m
$\chi(0,0)$		0.20
$T(0,0)$		66°C
$P(0,0)$		110 atm
$\rho(0,0)$	ρ_0	517.4 kg/m^3
$C^x(0,0)$		-1.71×10^{-7} kg/m·s
$C^T(0,0)$		1.55×10^{-10} kg/m·s°K
$C^P(0,0)$		-7.96×10^{-11} kg/m·atm·s
Horizontal temp. gradient,	T_x	1 K/300 m
Vertical temp. gradient,	T_z	−2 K/30 m
porosity	φ	25%
diffusion coefficient	D_{12}	1.02×10^{-9} m^2/s
viscosity	μ	200 kg/m·s

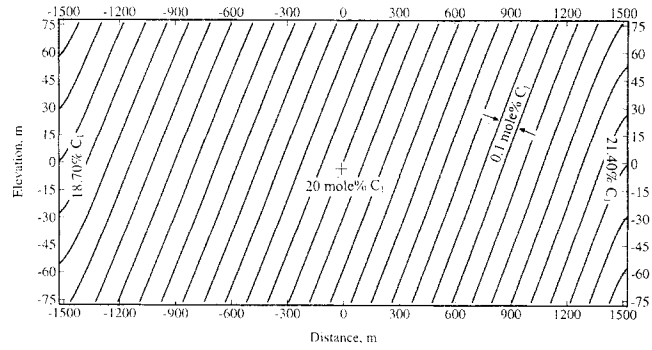

Figure 2. Methane mole fraction contours, $k = 0.06$ md—Example 1 ($\chi(0,0) = 20\%$).

Example 1: unaltered $C_1 - nC_4$ system

Since the compositional variation for zero permeability (that is, zero convection) is easily calculated, we used this as our starting point. This run requires only successive integration of Eq. 19 and the solution of Eq. 14. A contour plot of the methane mole fraction is shown in Figure 1. The contour interval is 0.1 mol%. In all subsequent composition plots we will use this same contour interval and in every case the mole fraction at the center of the reservoir will be 20%. This figure shows that the constant composition contours are essentially straight lines, indicating that the variation of the diffusion coefficients C^x, C^T and C^P is small. The contribution of ψ_j to this case is insignificant and setting $\psi_j = 0$ has no appreciable effect on the compositional variation. The horizontal compositional variation for $k = 0$ is 0.91 mol% at $z = 0$.

The procedure from then on was to increase the permeability and then iterate using the previous solution as the starting point. In this way we ran cases for $k = 0.003$, 0.01, 0.03, 0.06, 0.1, 0.2, 0.3, 0.5, 1.0, and 2.0 millidarcy (md). The behavior of the solution was not expected, nor did the iterative procedure work as well as we had hoped.

The surprise was that the increasing permeability had the effect of *increasing* horizontal compositional variation. Our expectation was that convection would decrease the compositional variation. Figures 1, 2 and 3 graph methane mole fraction contours for $k = 0.0$, 0.06 and 0.2 md. The horizontal variations in these cases are 0.91, 2.70 and 5.51 mol%, respectively. There are a few important points to note on these figures: (1) the contours are not only getting closer together —they are becoming more vertical; (2) except near the side boundaries, the curves seem to have the same shape and the spacing seems to be regular indicating that $\partial\chi/\partial x$ is roughly constant; (3) the curves are developing a subtle "s" shape which indicates that the vertical compositional gradient is not constant.

Up to this point, the iterative procedure worked well enough, although convergence slowed as permeability increased ($k = 0.2$ md required 50 iterations). The runs for higher permeabilities not only required more iterations, but also required that the rectangular grid be successively narrowed—$k = 2.0$ md required widths of 0.5 m at $\pm W/2$. Also, we could no longer take the full values of our updated guesses at each iteration step, but were forced to average them with the previous updates. In particular it was found that convergence was extremely sensitive to the vertically averaged horizontal potential gradient $\partial\bar{\phi}/\partial x$ given by Eq. 21. For the case of 2.0 md, we updated $\partial\bar{\phi}/\partial x$ using only 0.2% of the new iterate.

The compositional contours for $k = 0.5$ and 2.0 md are shown in Figures 4 and 5. The overall horizontal compositional variations for these are 4.25 and 1.94 mol%, respectively. The most important feature of these figures is that now the horizontal compositional gradients are *decreasing* with increasing permeability. They also show that these horizontal gradients are roughly constant away from the side boundaries. An interesting feature of Figure 5 is that the curves now have a negative slope near $z = 0$, indicating that

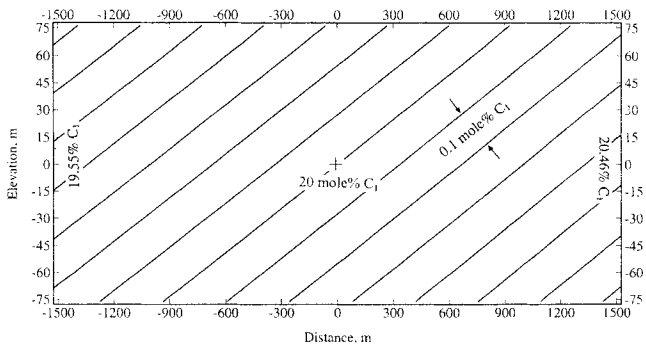

Figure 1. Methane mole fraction contours, $k = 0.00$ md—Example 1 ($\chi(0,0) = 20\%$).

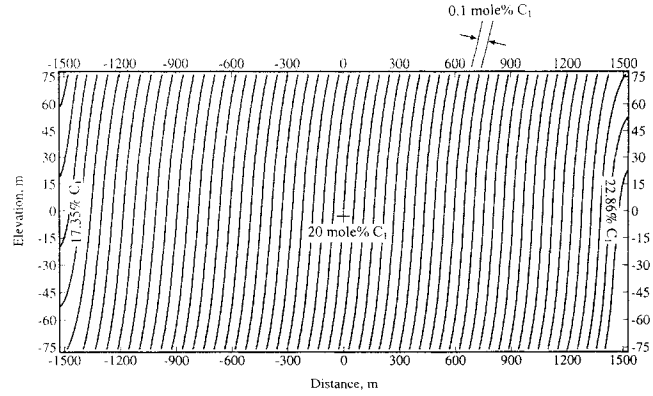

Figure 3. Methane mole fraction contours, $k = 0.2$ md—Example 1 ($\chi(0,0) = 20\%$).

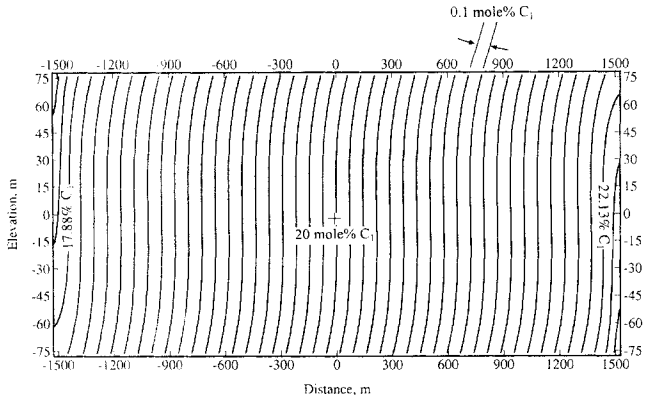

Figure 4. Methane mole fraction contours, $k = 0.5$ md—Example 1 ($\chi(0,0) = 20\%$).

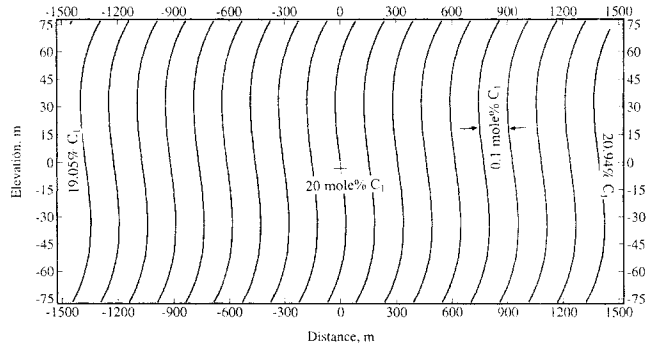

Figure 6. Methane mole fraction contours, $k = 2.0$ md, infinite rectangle—Example 1 ($\chi(0,0) = 20\%$).

the vertical concentration gradients are reversing sign in this region.

Up to this point, we assumed that the side boundaries had a significant effect on the horizontal gradients in the interior of the reservoir. We decided to check this in two ways. First, we reran some of the cases using a reservoir width of 300 m, rather than 3,000 m. Secondly, we removed the side boundaries.

In the case of the 300-m reservoir, we found the same behavior as before. Not only was the behavior in near $x = 0$ nearly identical for the two widths, but behavior near the side boundaries was the same at a given distance from those boundaries (that is, gradients at $x = 1{,}498.5$ m for the 3,000-m reservoir were nearly the same as at $x = 148.5$ m for the 300-m reservoir). In neither region did compositional gradients scale on width.

The success with the one 300-m reservoir, and the poor convergence using the 3,000-m reservoir encouraged us to try an infinite system. In this modification we performed our calculations on a 4,800-m reservoir using the same differentiated Green's functions without the images in $\pm W/2$. The width of the individual rectangles in this case were 150 m. At the edges of the reservoir, we added two rectangles that were each 3,000 m long and assigned the inhomogeneities in each to be identical to those in the adjacent block. The computations were performed as before on the 4,800-m core region with the only requirement being that the trends from the center 3,600 m were continued linearly outwards into each outlying 600 m section. It was hoped that in this way the center 3,000 m would behave as if it were part of an infinitely wide reservoir. We made no changes to the vertical geometry except for some minor modification of individual rectangle height.

No attempt was made to reproduce all of the earlier runs —we were more interested in determining the behavior for higher permeabilities than we were in seeing if an infinite system could be used for lower permeabilities. We did, however, rerun the 2.0-md case, shown in Figure 6. In this case the compositional change across the reservoir was 1.89 mol%. This compares favorably with the value of 1.94 mol% for the closed rectangle. Examination of Figure 6 shows no surprises; the behavior is essentially unchanged except near $\pm W/2$.

The iterative procedure now worked much better; not only did convergence require fewer iterations, but each iteration required less time. Typically, a single interation cycle took about 7–8 times more computation time for the closed rectangle than for the infinite rectangle. The number of iterations still increased and the weighting of $\partial\bar{\phi}/\partial x$ still needed to be decreased with increasing permeability. In addition to the 2.0 md run, runs for 5.0, 10, 30 and 100 md were also completed. The composition contours for 10, 30 and 100 md are shown in Figures 7, 8 and 9. These figures show the same general trend as before with the horizontal compositional changes being 0.55, 0.21 and 0.06 mol%. Note that in this range of permeabilities, these horizontal changes are roughly proportional to $1/k$.

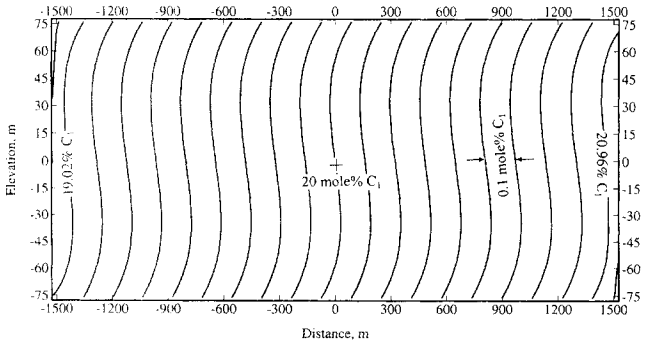

Figure 5. Methane mole fraction contours, $k = 2.0$ md, closed rectangle—Example 1 ($\chi(0,0) = 20\%$).

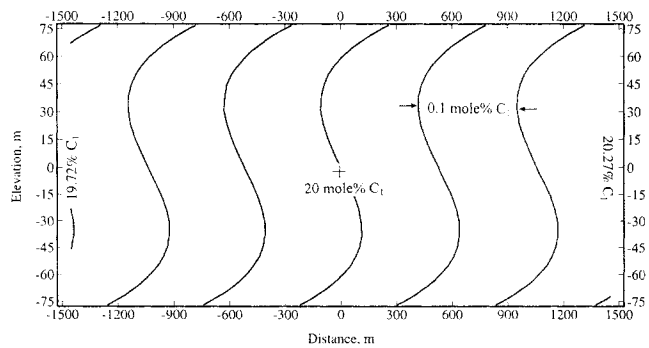

Figure 7. Methane mole fraction contours, $k = 10$ md—Example 1 ($\chi(0,0) = 20\%$).

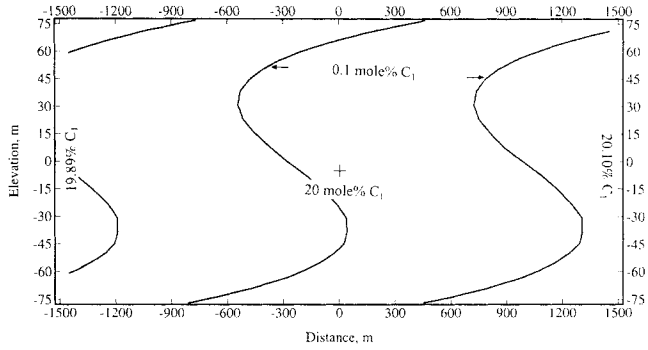

Figure 8. Methane mole fraction contours, $k = 30$ md—Example 1 ($\chi(0,0) = 20\%$).

We did not perform runs for higher permeabilities, because it was felt that we were straining the limits of our iterative method. Up to this point, the horizontal variation of composition was completely dominated by the horizontal averaged potential gradient, $\partial\bar{\phi}/\partial x$. Neither $\partial\psi_j/\partial z$ nor the exponential part of $\partial\phi/\partial x$ had any significant effect. Iterative solutions for higher permeabilities, however, would almost certainly exhibit regions of horizontal gradient reversal because these two components become more important. We do not believe that the true solution should exhibit these reversals and are unsure whether or where the solution technique is breaking down. It could be in the way we are approximating the infinite reservoir or in the numerical computation of $\nabla \times \psi_j$. It may even be something as mundane as the loss of significance in our Green's function integrals. We do not anticipate the emergence of different behaviors for higher permeabilities, but different regimes may exist. This problem is currently under investigation. Up to 100 md, we have confidence in our method because it is confirmed by the perturbation solution we developed analytically. The perturbation solution will be discussed later.

So far, we have only presented plots of composition. We could possibly have made better arguments by showing potential gradients, flow lines and localized behaviors, but for the sake of brevity we show a few figures for completeness. This is also because knowledge of their behavior enhances the arguments we make in the development of the perturbation solution.

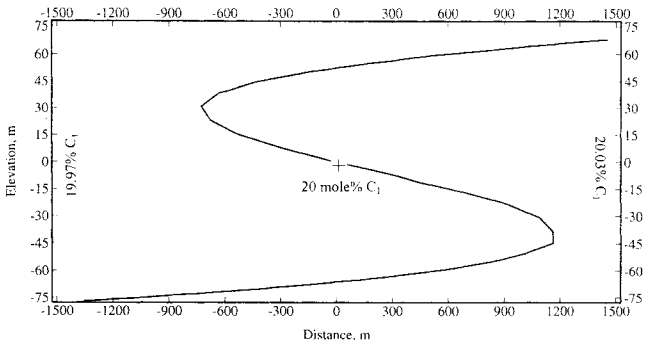

Figure 9. Methane mole fraction contour, $k = 100$ md—Example 1 ($\chi(0,0) = 20\%$).

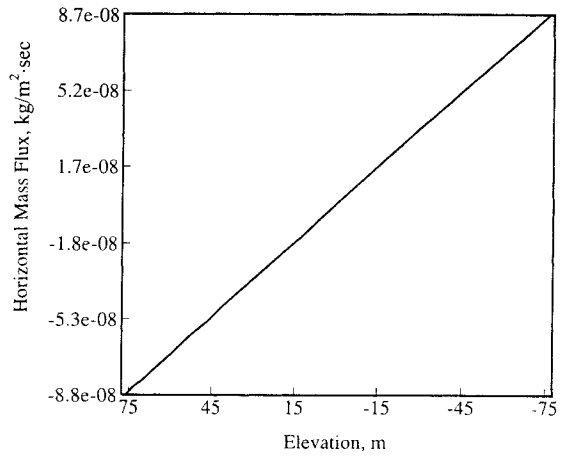

Figure 10. Total horizontal mass flux, $k = 2.0$ md, at $x = 0$—Example 1.

Figure 10 shows the horizontal component of total mass flux ρv_x at $x = 0$. This figure shows the case of the finite rectangle for $k = 2.0$ md, but the qualitative behavior is the same for all permeabilities whether the rectangle is finite or unbounded. The important feature of this plot is that ρv_x is essentially a linear function of elevation. This velocity profile is closely approximated by $(kg/2\varphi\mu)(\partial\rho^2/\partial x)z$ which is the solution to Eq. 13, assuming the right side to be constant. A few important points regarding the horizontal mass flux (at least away from the side boundaries) are: (1) it is orders of magnitude greater than the vertical mass flux ρv_z; (2) it is very weak function of x; and (3) the flow field in the reservoir consists of one large convective cell.

Figure 11 shows a vertical slice of $\partial\phi/\partial z$ (at $x = 0$ for the same run), which accounts for nearly all of the vertical variation of composition. This figure shows that the vertical gradient of composition is roughly proportional to $(z^2 - H^2/4)$. Recall that $\partial\chi/\partial z$ is given by $(-\partial\phi/\partial z + \partial\psi_j/\partial x - C^T\partial T/\partial z - C^P\partial P/\partial z)/C^\chi$. Here the ψ_j term is negligible while the sum of the pressure and temperature terms is approximately equal to 4.9×10^{-12} kg/m^2·s. This means that a reversal in vertical

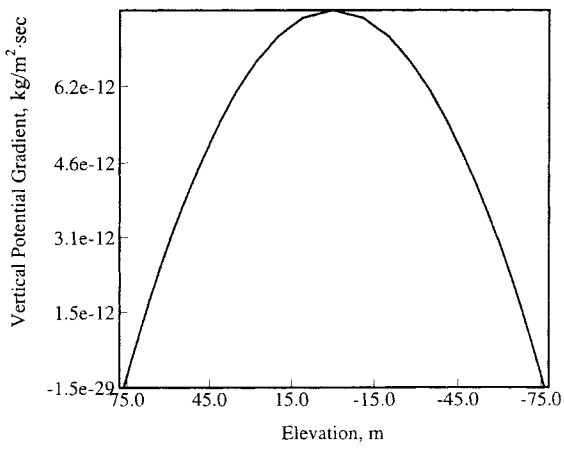

Figure 11. Vertical potential gradient, $k = 2.0$ md, at $x = 0$—Example 1.

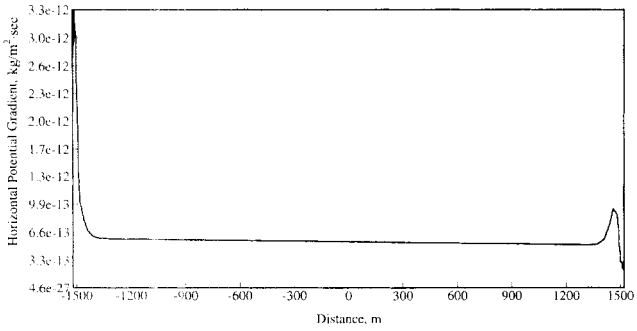

Figure 12. Horizontal averaged potential gradient, k = 2.0 md, closed rectangle—Example 1.

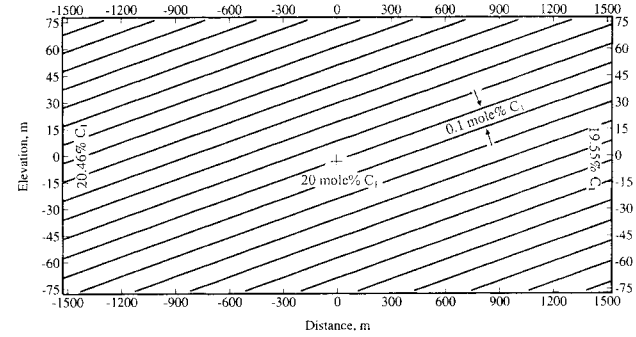

Figure 13. Methane mole fraction contours, k = 0.00 md—Example 2 ($\chi(0,0)$ = 20%).

composition gradient occurs at $z \cong \pm 30$ m. This agrees with the composition profiles shown in Figures 5 through 9.

Figure 12 shows the vertically-averaged horizontal potential gradient $\partial\bar{\phi}/\partial x$ for the closed rectangle and $k = 2.0$ md. This figure shows the boundary layers at the two ends. The existence of boundary layers in a binary system of nitrobenzene-hexane with horizontal temperature gradient has been observed recently by Platten and Chavepeyer (1995). The local maxima near the boundaries require some discussion. The reason for these maxima is unclear, but they seem to develop only for permeabilities where $\partial\chi/\partial x$ decreases with rising permeabilities (in this example, for permeabilities greater than 0.2 md). Their magnitudes seem to be a slowly decreasing function of permeability, while their widths and distances from the boundaries are roughly proportional to $1/k$. These maxima do not develop when the reservoir is taken to be infinitely wide.

We have no explanation for the existence of these maxima, but the fact that these boundary layers do exist has two important implications. The drawback is that it limits the usefulness of the iterative technique: the grid needs to be highly refined in these regions and the rate of convergence is slowed greatly. The benefit is more philosophical—the velocities and compositions in the boundary layers seem to arrange themselves so as to consume the horizontal boundary condition; the boundary conditions at $x = \pm W/2$ only affect behavior in the boundary layers and that the region between the maxima is independent of the boundary conditions. Note that in the central part of the reservoir the potential gradient has a gently sloping linear trend. This trend is almost identical to that for the case of $k = 2.0$ md in an infinite rectangle.

Example 2: $C_1 - nC_4$ system, reversed thermal diffusion

In this example we consider the same case as before, but change the sign of k_T and, therefore, the sign of the entire C^T term; as a consequence, the methane concentrates in the colder regions. This is an important difference because in Example 1 the vertical pressure and thermal effects competed and the thermal effects dominated.

Another important difference here is that the horizontal density-squared gradient is a combination of two competing effects—the thermal component $(\partial\rho^2/\partial T)(\partial T/\partial x)$ is now opposite in sign to $(\partial\rho^2/\partial\chi)(\partial\chi/\partial x)$. Recall that Eq. 13 indicates that velocities are proportional to the permeability and the horizontal density-squared gradient; in this example, the density gradient will decrease as the permeability increases. This is in line with the observations of Jacqmin (1986, 1990), Moser (1986), and Chavepeyer and Platten (1994) and is apparently well known.

Figure 13 shows the starting point for this set of iterations $k = 0$. This presentation is the same as before: the contour lines show equal values of methane mole fraction, the contour spacing is 0.1 mol%, and the composition at the center of the reservoir is assigned to be 20 mol% methane. The significant feature of this figure is that now the methane concentration is highest at the top of the reservoir. The total horizontal compositional difference is -0.91 mol%. This value has the same magnitude as Example 1, but the sign is changed. Figure 14 shows the density contours for this case. (The contour interval is 0.16 kg/m^3 and the value at the center is 517.4 kg/cm^3. This interval and reference density are maintained in the next two density plots.) The magnitude of the density is not important, but the slope of the contours is. These slopes are equal to $-(\partial\rho/\partial x)/(\partial\rho/\partial z)$. In all of the cases we will show, the vertical density gradients are positive throughout the reservoir, so in Figure 14 the horizontal density gradients are negative.

Figure 15 shows the composition profiles for $k = 0.1$ md. These profiles are similar to those of Figure 13 and the horizontal composition difference is now -1.81 mol%. Figure 16 shows the density contours. Here, again, all of the vertical gradients are positive. The horizontal gradients are still negative, although they have decreased in magnitude. In this case the mass flux exhibits one large convective cell, a vertical

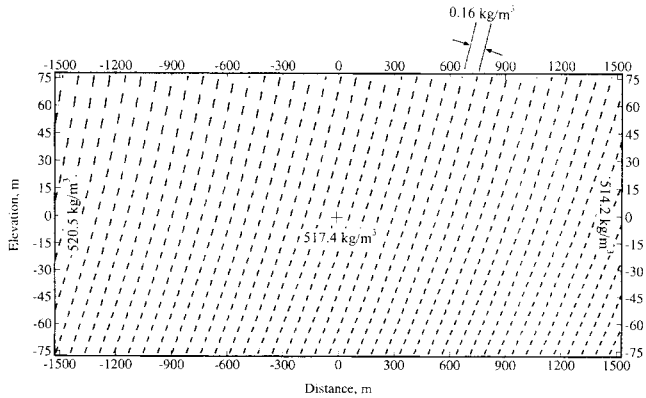

Figure 14. Density contours, k = 0.00 md—Example 2 ($\rho(0,0)$ = 517.4 kg/m^3).

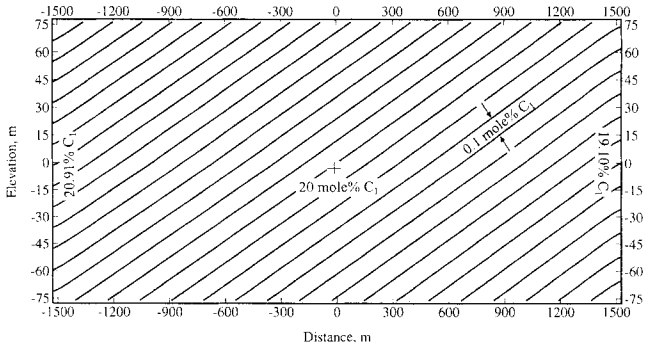

Figure 15. Methane mole fraction contours, $k = 0.1$ md—Example 2 ($\chi(0,0) = 20\%$).

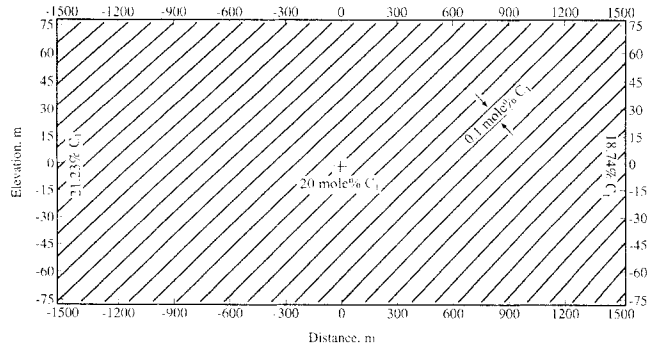

Figure 17. Methane mole fraction contours, $k = 100$ md—Example 2 ($\chi(0,0) = 20\%$).

slice of horizontal mass flux is roughly approximated by $(kg/2\varphi\mu)(\partial\rho^2/\partial x)z$, and the vertical potential gradient at $x = 0$ is roughly parabolic. These three phenomena are consistent with those of Example 1.

There is very little change in composition for this example as the permeability is increased; we show only the case, $k = 100$ md—the limit of our calculations. Figure 17 shows the compositional contours. They are essentially the same as in Figure 15, except that now the horizontal change is -2.49 mol %.

The reason that the compositions have changed so slowly is that the horizontal density gradient is decreasing. This much was expected, but the manner in which it occurred was not. Figure 18 shows the density contours for this case. Note that above the centerline $z = 0$, the slope is predominantly negative, while below it is predominantly positive. This indicates that a second convective cell should exist, and it does. Figure 19 shows ρv_x at $x = 0$. Here the horizontal mass flux is zero at two points, is negative in the center, and positive at the top and bottom. The vertical potential gradient $\partial\phi/\partial z$ is now no longer parabolic, but develops two local extrema, as shown in Figure 20. Figure 21 shows $\partial\bar{\phi}/\partial x$ for $k = 0.1$ md. This figure does not show the local maxima that Figure 12 showed. We believe this is because the horizontal concentration gradient is still steepening. Figure 21 does show, however, a steep rise to a region of linear behavior. This region of rapid rise is a boundary layer and narrows as permeability increases in much the same way as in the Example 1.

We did not proceed to higher permeabilities, so we cannot predict their behavior with a high degree of certainty. The two convective cells that are present for $k = 100$ md seem to have stabilized, since the qualitative nature of the density and velocity fields is essentially unchanged from that of $k = 10$ md. However, we cannot guarantee that the reservoir will not break in two as permeability is increased—there is a possibility that the two convective cells will act independently of each other, forming an imaginary barrier at $z = 0$ and exhibit opposite behavior in each cell. There is also the possibility that the two cells will break into four and those four into eight, and so on. This last possibility seems to be the least likely of the three.

Perturbation Analysis

We have reached a point where the main problem can be tackled—predicting horizontal compositional variation. We can do this, because we now have a good idea of the behavior from our iterative solution examples. The perturbation scheme we pursue is simple and does an excellent job of predicting these variations except in the boundary layers. The analysis is done in two stages: first we develop a cubic equation that gives the variation at $x = 0$, and second we integrate this horizontally to determine the variation as a function of x.

Analysis at x = 0

The gist of the method is to assume that $\partial\chi/\partial x$ is constant and to determine it from $\partial\bar{\phi}/\partial x$ given by Eq. 21 of the last section (which we reprint here)

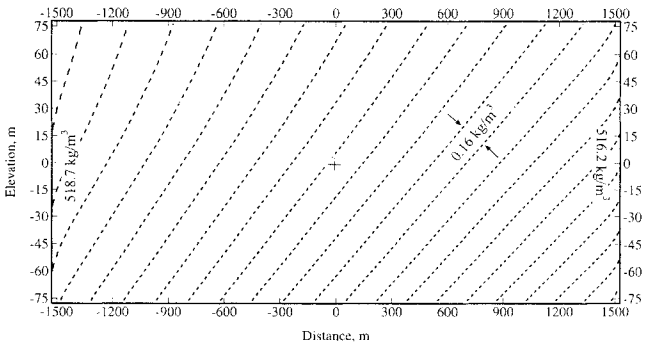

Figure 16. Density contours, $k = 0.1$ md—Example 2 ($\rho(0,0) = 517.4$ kg/m^3).

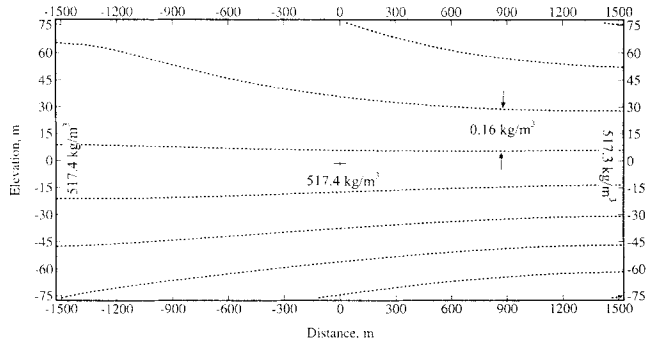

Figure 18. Density contours, $k = 100$ md—Example 2 ($\rho(0,0) = 517.4$ kg/cm^3).

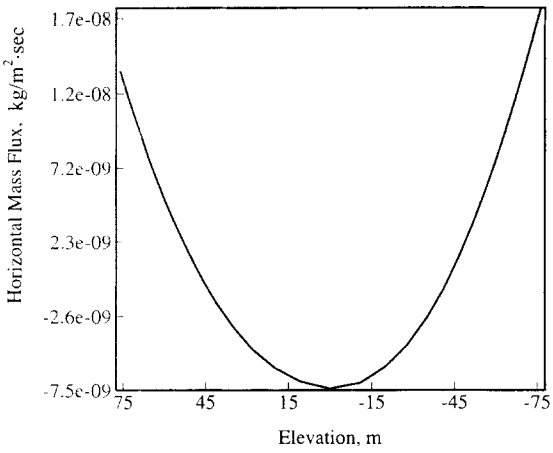

Figure 19. Total horizontal mass flux, $k = 100$ md, at $x = 0$—Example 2.

$$\frac{\partial \overline{\phi}}{\partial x} = \frac{1}{H}\int_{-H/2}^{H/2} \omega \rho v_x dz. \tag{22}$$

This requires that we approximate the flow field and the vertical variation of weight fraction. Jacqmin (1990) uses the same procedure we outline below except that he sets this integral equal to zero rather than $\partial\overline{\phi}/\partial x$ (and does not consider thermal diffusion).

Here we assume that the effects of the lateral boundaries are insignificant and that the $\partial\chi/\partial x$ is neither a function of x or of z. We assume that all of the diffusion coefficients are constant, as are the partial derivatives of ρ^2 with respect to composition and temperature. We also assume that density is not a function of z and that the pressure gradient is given by $\nabla P = -\rho_0 g\hat{z}$. We also assume that permeability, viscosity, porosity and temperature gradients are constant, as before.

It is convenient here to work with the weight fraction as opposed to the mole fraction, and so we rewrite the diffusive flux as

$$-\nabla\phi = C^{\omega}\nabla\omega + C^{T}\nabla T - C^{P}\rho_0 g\hat{z}. \tag{23}$$

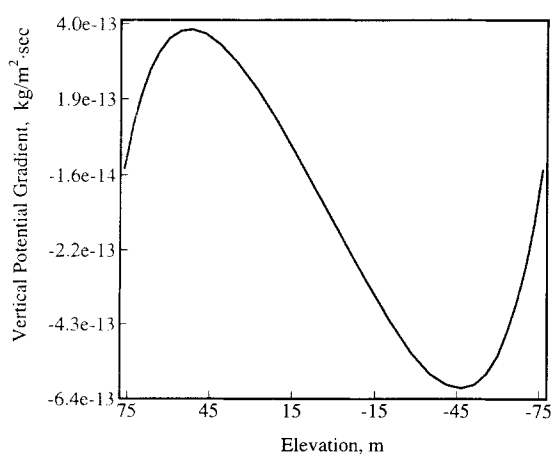

Figure 20. Vertical potential, $k = 100$ md—Example 2.

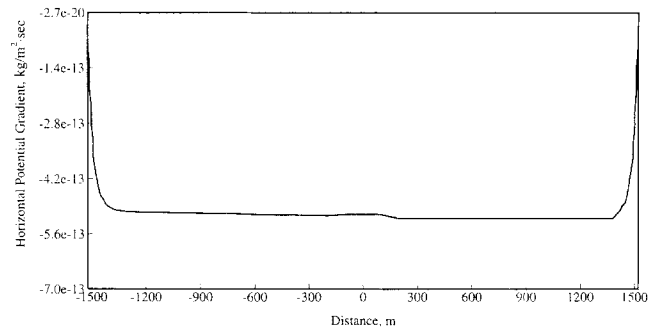

Figure 21. Horizontal averaged potential gradient at $k = 0.1$ md—Example 2.

Note that C^{ω} is equal to $C^{x}d\chi/d\omega$, and that because the diffusion coefficients are now constant, the rotational part of $\vec{j}$ is zero.

The first quantity we need is mass flux from Eq. 13. Since the right side of this equation is constant and we are not imposing any horizontal boundary conditions, the solution requires only a single integration

$$\rho v_x = -\frac{\partial\psi}{\partial z} = \frac{kg}{2\varphi\mu}\rho_x^2 z = \frac{kg}{2\varphi\mu}(\rho_\omega^2\omega_x + \rho_T^2 T_x)z. \tag{24}$$

The subscripts on the right side of this equation denote differentiation. The subscripts on density-squared denote the derivatives of density-squared and not the squares of the derivatives. Note that to this order, there is no vertical component of velocity.

The determination of weight fraction as a function of elevation requires we find $\partial\phi/\partial z$. The assumptions above imply that ϕ is a linear function of x. Therefore, its second-x derivative must be zero. So, we find $\partial\phi/\partial z$ by integrating Eq. 16 in the form

$$\frac{\partial^2\phi}{\partial z^2} = \frac{kg}{2\varphi\mu}\omega_x\rho_x^2 z, \tag{25}$$

which yields

$$\frac{\partial\phi}{\partial z} = \frac{kg}{2\varphi\mu}\omega_x\rho_x^2\left(\frac{z^2}{2} - \frac{H^2}{8}\right). \tag{26}$$

Using this expression in Eq. 23 gives

$$\omega(0,z) = \omega(0,0) - \frac{kg}{2\varphi\mu}\frac{\omega_x\rho_x^2}{C^{\omega}}\left(\frac{z^3}{6} - \frac{H^2 z}{8}\right) + \left(\frac{C^P}{C^{\omega}}\rho_0 g - \frac{C^T}{C^{\omega}}T_z\right)z. \tag{27}$$

Now we need only insert this expression for weight fraction and the expression for mass flux into Eq. 22, and integrate and set the result equal to the horizontal component of Eq. 23. The result of these steps is a cubic equation for ω_x

$$\left(\frac{kg}{2\varphi\mu}\right)^2 \frac{H^4}{120} \frac{(\rho_\omega^2\omega_x + \rho_T^2 T_x)^2 \omega_x}{(C^\omega)^2}$$

$$+\left(\frac{kg}{2\varphi\mu}\right)\frac{H^2}{12}\frac{(\rho_\omega^2\omega_x + \rho_T^2 T_x)}{C^\omega}\left(\frac{C^P}{C^\omega}\rho_0 g - \frac{C^T}{C^\omega}T_z\right)$$

$$+\left(\omega_x + \frac{C^T}{C^\omega}T_x\right) = 0. \quad (28)$$

We choose to present the final equation for ω_x in this form, because it more clearly brings out the important aspects of the solution. Note that the term $(\rho_\omega^2\omega_x + \rho_T^2 T_x)$ represents the horizontal density-squared gradient, and the term $(C^P/C^\omega\rho_0 g - C^T/C^\omega T_z)$ is the vertical compositional gradient for the case of zero permeability. This last term can be considered a buoyancy term including both temperature and pressure effects. If we follow the steps in Jacqmin (1990) and include thermal diffusion, we get Eq. 28 without the term $\omega_x + C^T/C^\omega T_x$.

A review of the steps in the perturbation analysis shows that it closely matches the behavior of Example 1: the mass flux is proportional to z, and the vertical potential derivative $\partial\phi/\partial z$ is parabolic. This solution is, therefore, expected to be a good approximation to ω_x for Example 1 at the origin. Figure 22 shows the horizontal derivative of mole fraction at $x = 0$, $z = 0$ for the iterative solution of Example 1, and the solution of the cubic above. The agreement is excellent with the greatest discrepancy being less than 1%. We also include on this figure our modification (that is, the inclusion of thermal diffusion) of Jacqmin's solution. Note that his solution asymptotes to ours as permeability approaches infinity, where the term he neglects becomes unimportant.

The close agreement in the case of Example 1 is encouraging. However, it is not that surprising, since each step in the perturbation solution exhibited the same behavior as the iterative solution. We were surprised to find close agreement for

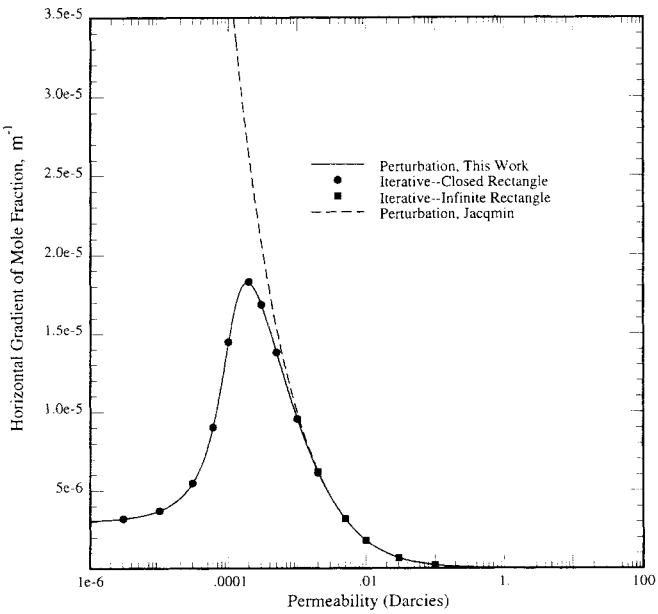

Figure 22. Horizontal mole fraction gradient at $x = 0$, and $z = 0$—Example 1.

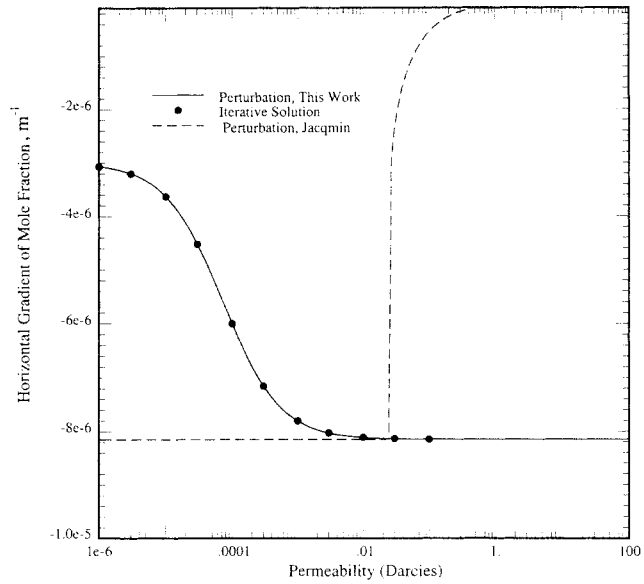

Figure 23. Horizontal mole fraction gradient at $x = 0$, and $z = 0$—Example 2.

Example 2, shown in Figure 23. In fact, the agreement is much closer than before, the maximum deviation being slightly less than 0.1%. This is surprising because Example 2 exhibits neither a mass flux profile proportional to z nor a parabolic $\partial\phi/\partial z$ profile. Apparently, the fact that $(\rho_\omega^2\omega_x + \rho_T^2 T_x)$ approaches zero is more important than the mass flux profile or vertical potential derivative. Here also we include our modification of Jacqmin's solution. His solution does not match the data nearly as well as in Example 1; the neglected term plays an important role for all permeabilities.

Extension to $x \neq 0$

Extension of the perturbation scheme to other values of x can readily be made. Note, we assumed C^ω, C^T, C^P, ρ_0, and so on were constant and assigned their values using the values of χ, T and P given at the origin. Recall that we are given temperature at all points in the reservoir, pressure changes very little horizontally, and, using Eq. 28, we now have a good approximation for χ at $x = \pm\Delta x$. So, in principle, we can step out at will to either the right or the left, resolve the cubic with new parameters, and continue stepping indefinitely.

Figure 24 shows the comparison of this perturbation solution with the iterative solution for the closed rectangle in Example 1 with $k = 2.0$ md. Note that the agreement is excellent except in the boundary layer region.

Explaining the horizontal gradient

We have seen that perturbation solution accurately predicts the horizontal compositional gradients, at least at $z = 0$. We can also use the perturbation concept to answer the question: "Why does a small amount of convection cause horizontal composition gradients?" The argument is simplified greatly if we assume that there is no thermal diffusion.

If we consider a rectangular reservoir where $C^T = 0$, and where C^χ and C^P are not functions of temperature, then the static compositional variation will be purely vertical (that is, the horizontal compositional gradient will be zero). A repre-

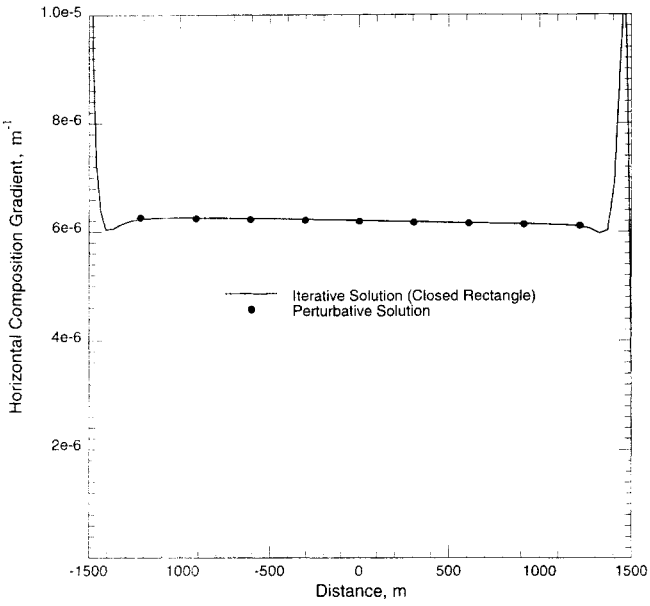

Figure 24. Compositional gradient at $z = 0$, $k = 2.0$ md—Example 1.

sentation of the vertical grading is shown by the solid curve A of Figure 25a (the dashed line shows zero vertical grading). So far, we have not violated the conservation of mass constraint because there is no convection. Now consider that the permeability is increased so that there is a small amount of ρv_x that is proportional to z, as shown by solid curve B (the dashed line shows zero convection), and that ρv_z is identically zero. We now have violated our material balance constraint for component one since $\int_{-H/2}^{H/2} \omega \rho v_x dz$ (that is, the integral of the product of curves A and B) is not zero. There will be more of component one moving to the right than to the left and hence a buildup of component one. In order for this not to happen, either the compositions must redistribute vertically (see curve C) or $\int_{-H/2}^{H/2} \omega \rho v_x dz + \int_{-H/2}^{H/2} j_x dz = 0$. The integral $\int_{-H/2}^{H/2} j_x dz$ represents the contribution of horizontal diffusion (and hence some horizontal compositional gradient).

We can think of Eq. 28 as a function of permeability. When viewed in this way, each of the three terms corresponds to a different part of the material balance argument. The k^0 term corresponds to completely static conditions; since $\partial P/\partial x$ is

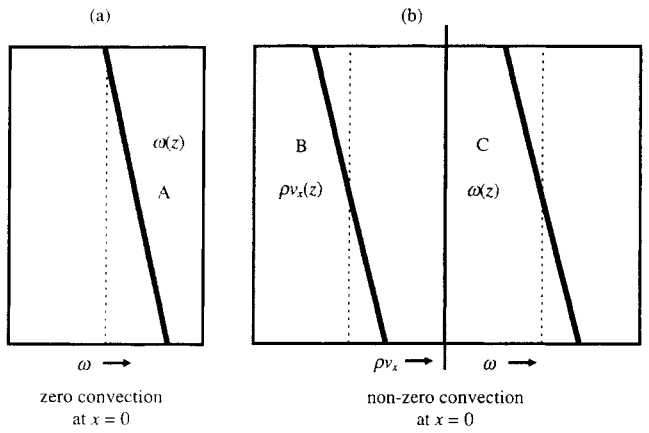

Figure 25. Material balance arguments.

insignificant, the horizontal gradient is due to thermal diffusion. The k^1 term represents the horizontal diffusion that balances the convective flux in the absence of vertical compositional redistribution. The k^2 term gives the further deviations in horizontal gradient caused by redistribution of vertical composition profile. Note that Jacqmin's approach implicitly assumes that the material balance error caused by convection is completely accounted for by redistribution vertically.

Further examination of the perturbation solution

An investigation of Eq. 28 gives some important generalizations of the phenomenon seen in the two examples already discussed. For instance, it clearly shows that the solution scales as the product of permeability and thickness *squared.* This means that reducing the thickness by a factor of two will result in the curves of Figures 22 and 23 being shifted to the left by a factor of four, without changing their shape. The cubic equation also shows that as k approaches zero, the solution asymptotes to $-C^T/C^\omega T_x$ and that ω_x decays as $1/k$ as permeability approaches zero (if the density derivative is not zero).

A closer examination of the cubic equation reveals that ω_x can have at most two extrema—one occurring at intermediate values of k and the second at $k = \infty$ (whose value must be zero, if the first extrema occurs). Therefore, Figure 22 exhibits all of the possible qualitative behavior predicted by the cubic equation. Of course, all of these features need not develop. The most significant deviation occurs if $\rho_\omega^2 \omega_x$ becomes equal to $-\rho_T^2 T_x$, as was the case in Example 2.

Let us examine the "hump" in Figure 22. Note that for low permeabilities the order k^0 and k^1 terms dominate. The hump develops when the k^2 term begins to dominate the k^0 term. Prior to this, the value $\omega_x = 0$ is in no way distinguished. This means that there is no reason that the gradient could not start at a negative value, say, increase straight through $\omega_x = 0$, reverse sign, and then reach a local maxima. This behavior requires no contrivance, but merely values of C^T, C^P, and so on that seem no less likely than any others. Also note that thermal diffusion has little effect on the qualitative behavior—it affects only the asymptote as permeability approaches zero and the position and height of the hump through the buoyancy term $(C^P/C^\omega \rho_0 g - C^T/C^\omega T_z)$.

The question is: What happens in the case of a multicomponent fluid? In the case of an n-component single-phase fluid, there will be: $n-1$ equations corresponding to Eq. 23, one equation of the type of Eq. 24, and $n-1$ equations of the type Eq. 28. The result will be $n-1$ cubic equations, which need to be solved simultaneously. This may or may not be a simple task, but it will be much easier than solving the corresponding differential equations with the iterative method.

We need to emphasize again an important point. Everything we have done in this section was predicated on the assumption that Examples 1 and 2 exhibited all of the behavior that would arise as permeability increases to infinity. It is possible that other regimes will develop for higher permeabilities. This possibility needs to be investigated.

Discussion and Conclusions

This work investigates the compositional variation of a single-phase, two-component system due to the combined ef-

fects of natural convection and diffusion. Our goal was to develop simplified solutions that would give us accurate compositions at all points under all conditions, but the main objective was in the horizontal compositional distributions.

The investigation was made much more difficult, because we did not know the most basic effects that convection would have on composition. We embarked on a simple iterative method in order to include virtually all of the fluid property variations. It would have been nice if this procedure converged quickly for all cases—but it did not. However, we were able to force it to work well enough to give us a good idea how the solutions behaved.

The real value of this work is that we were able to use those discovered behaviors to motivate a perturbation solution that not only gives very accurate horizontal compositional variations, but also clearly indicates the interplay of the various parameters.

The major findings of interest are:

(1) The vector formulation introduces new variables, which are related to bulk velocity and composition.

(2) Increasing permeability normally does *not* cause a monotonic lessening of horizontal compositional variation. Often, there is a local maximum/minimum in gradient, when considered as a function of permeability. This local extremum may be of either sign and either greater or less than the initial ($k = 0$) gradient. If this local extremum develops, the compositional gradient then lessens monotonically to zero as permeability approaches infinity. In this final stage the gradient decays as $1/k$.

(3) The only case where a local maximum does not develop is when the horizontal density gradient due to temperature cancels that due to composition. This causes the horizontal compositional gradient to asymptote to a nonzero limiting value without attaining a maxima or minima. A series of runs with the iterative model indicates that two cells spanning the width of the reservoir develop at high permeabilities in this case. The perturbation solution does not predict these two cells, yet gives very good values for horizontal compositional gradient.

(4) Thermal diffusion plays an important role in the qualitative behavior of the horizontal compositional variation. It accounts for the magnitude of the horizontal gradient as permeability approaches zero, and affects the height and location of the maxima/minima through the pressure/temperature buoyancy term. It also affects the direction of convection.

(5) Boundary layers develop at the right and left boundaries of the reservoir and decrease in width as permeability increases. Within these regions there is rapid change in compositional gradients which seem to consume the right and left boundary conditions. This leaves a large region in between where the effects of the boundaries are insignificant.

(6) The perturbation method applied to an n-component system will require the simultaneous solution of $n-1$ cubic equations.

The above conclusions assume that the behavior found using the iterative procedure is exhaustive. However, this procedure was not able to investigate cases of high permeabilities. There is a possibility that other compositional regimes develop as permeability approaches infinity. This possibility needs to be investigated.

Notation

c_p = heat capacity at constant pressure
C^x = coefficient of mole fraction gradient in $\vec{j}$
C^ω = coefficient of weight fraction gradient in $\vec{j}$
C^P = coefficient of pressure gradient in $\vec{j}$
C^T = coefficient of temperature gradient in $\vec{j}$
M_i = molecular weight of component i
P = pressure
ρ_0 = fluid density at $x = 0$, $z = 0$
$\rho_T^2 = \partial\rho^2/\partial T$
$\rho_x^2 = \partial\rho^2/\partial x$
$\rho_\omega^2 = \partial\rho^2/\partial\omega$
ϕ = irrotational part of $\omega\rho\vec{v}$ and $-\vec{j}$
ψ = stream function
ψ_j = rotational part of $\vec{j}$
ψ_{v1} = rotational part of $\omega\rho\vec{v}$
$\omega_x = \partial\omega/\partial x$

Acknowledgments

This work was supported by the members of the research consortium on fractured and layered reservoirs of the Reservoir Engineering Research Institute and the U.S. DOE grant DE-FG22-93BC14875. Their support is greatly appreciated.

Literature Cited

Bird, R. B., W. E. Stewart, and E. N. Lightfoot, *Transport Phenomena*, Wiley, New York (1960).

Bedrikovetskii, P. G., D. G. Polonskii, and A. A. Shapiro, "Analysis of the Convective Instability of a Binary Mixture in a Porous Medium," Translated from *Izvestiya Rossiiskoi Akademii Nauk, Mekhanika Zhidkosti i Gaza*, No. 1, 110 (Jan/Feb 1993).

Borisenko, A. I., and I. E. Tarapov, *Vector and Tensor Analysis with Applications*, Dover Publications, New York (1979).

Chavepeyer, G., and J. K. Platten, "Effet de la Thermodiffusion sur la Separation de Phase en Condition de Non-Equilibre (Thermal Diffusion Effect on Phase Separation in Nonequilibrium Condition)," *Entropie*, 184/185, 27 (1994).

Firoozabadi, A., *Advanced Thermodynamics of Hydrocarbon Reservoirs*, McGraw-Hill, New York (1998).

Jacqmin, D., "Convection of a Gravity Segregating Fluid Forced by a Horizontal Temperature Gradient: An Energy Stability Analysis," *Mathematics Applied to Fluid Mechanics and Stability*, SIAM Press, Philadelphia, p. 263 (1986).

Jacqmin, D., "Interaction of Natural Convection and Gravity Segregation in Oil/Gas Reservoirs," *SPERE*, p. 233 (May, 1990).

Lu, Pau-Chang, *Introduction to the Mechanics of Viscous Fluids*, Holt, Rinehart and Winston, New York (1973).

Moser, R. D., "Mass Transfer by Thermal Convection and Diffusion in Porous Media," paper presented at the 1986 Intl. Conference on Applied Mechanics (Oct. 1986).

Peng, D. Y., and D. B. Robinson, "A New Two-Constant Equation of State," *Ind. Eng. Chem. Fund.*, **15**, 59 (1976).

Perkins, T. K., and O. C. Johnston, "A Review of Diffusion and Dispersion in Porous Media," *Soc. Pet. Eng. J.*, 70 (March 1963).

Platten, J. K., and G. Chavepeyer, "Phase Separation under a Temperature Gradient," *Physica A*, **213**, 110 (1995).

Rutherford, W. M., and J. G. Roof, "Thermal Diffusion in Methane n-Butane Mixtures in the Critical Region," *J. Phys. Chem.*, **63**, 1506 (1959).

Sigmund, P. M., "Prediction of Molecular Diffusion at Reservoir Conditions: Measurement and Prediction of Binary Dense Gas Diffusion Coefficients," *JCPT*, 48 (Apr.–June, 1976).

Shukla, K., and A. Firoozabadi, "A New Model of Thermal Diffusion Coefficients in Binary Mixtures," *I&EC Res.*, in press (1997).

Manuscript received May 12, 1997, and revision received Oct. 28, 1997.